


Topological edge/corner states and polaritons in dimerized/trimerized superconducting qubits in a cavity

Motohiko Ezawa 

Department of Applied Physics, University of Tokyo, Hongo 7-3-1, 113-8656, Japan



(Received 4 September 2023; revised 26 April 2024; accepted 7 May 2024; published 17 May 2024)

We investigate a two-level topological system with an alternating XX coupling in a photon cavity. It is mapped to a free boson model equally coupled to a photon, whose interaction is highly nonlocal. We analyze the Su-Schrieffer-Heeger model and the breathing kagome model. Intriguing phenomena occur in the topological phase due to hybridization between the photon field and the topological edge or corner state. As the photon coupling increases, the symmetric edge or corner state is smoothly transformed into a polariton state coupled with the edge or corner state. Simultaneously, the photon state is smoothly transformed into the symmetric edge state or the C_3 -symmetric corner state. Furthermore, a state is detached from the bulk band and smoothly transformed into a polariton due to hybridization with the photon field.

DOI: [10.1103/PhysRevB.109.205421](https://doi.org/10.1103/PhysRevB.109.205421)

I. INTRODUCTION

Topological insulator is a fascinating concept found in condensed-matter physics [1,2]. A simplest example is the Su-Schrieffer-Heeger (SSH) model, where topological edge states emerge in the topological phase. Higher-order topological insulator is an extension, where topological corner states emerge in the topological phase [3–9]. The breathing kagome model is one of the simplest models of higher-order topological insulators [9].

Cavity quantum-electrodynamics (QED) is a field of studying the coupling effect between atoms with discrete levels and a photon [10–14]. For example, by placing two mirrors in parallel, the energy of photon is quantized and cavity QED is realized. Cavity QED is also realized in superconducting qubits based on Josephson junctions [15,16]. The coupling constant between the discrete levels and a photon can be largely enhanced experimentally [17–22]. Then, a polariton emerges, which is a quasiparticle where the photon field is strongly coupled with another degree of freedom. Polaritons and related bound states in a cavity QED have been studied in variety of contexts [23–27].

Recently, cavity quantum materials attracted much attention [28], where a material instead of an atom is deposited in the mirrors. Superconductivity [29], ferroelectricity [30], photon-magnon coupling [31], and quantum Hall effects [32–34] are studied in the context of cavity quantum materials. A fermionic SSH model coupled with a photon is studied [35–38]. Topological properties of interacting atoms in the cavity are also discussed [39–43], where superconducting qubits enable us to realize strong interatomic couplings [40,41].

In this paper, we investigate the topological zero-energy edge and corner states in cavity-coupled arrays of an interacting two-level system. It is mapped to a hopping model with an additional site representing a photon, which couples to all of the other sites equally. We analyze a dimerized one-dimensional chain and a breathing kagome model with alternating XX interactions. They are shown to be mapped

to the SSH model and the breathing kagome second-order topological insulator model coupled with an additional photon site, respectively. When the coupling with the cavity increases, intriguing phenomena occur due to hybridization between the photon field and the topological edge or corner state. The symmetric edge or corner state is smoothly transformed into a polariton. Simultaneously, the photon state is smoothly transformed into the symmetric edge state or corner state. On the other hand, the other topological edge state or corner states remain as they are because they do not couple with the photon. Furthermore, another polariton emerges due to hybridization between the photon field and a state detached from the bulk bound. Thus, we have two types of polaritons, each of which is found to have the photon number 1/2 when the coupling with the cavity is sufficiently large.

This paper is composed as follows. We introduce a Hamiltonian describing cavity-coupled two-level systems in Sec. II. Photon loss effects are introduced in Sec. III. We study a cavity-coupled SSH model in Sec. IV and a cavity-coupled breathing kagome model in Sec. V. Section VI is devoted to discussions.

II. CAVITY PSEUDOSPIN SYSTEM

We consider a system made of N qubits equally coupled with one photon. With the use of the rotating wave approximation, cavity QED with the XX interaction is described by

$$H_{\text{total}} = \hbar\omega_0 \hat{a}^\dagger \hat{a} + H_{\text{spin}} + \hbar g \sum_{\alpha=1}^N (\hat{a}^\dagger \sigma_{\alpha}^{-} + \hat{a} \sigma_{\alpha}^{+}), \quad (1)$$

where $\hbar\omega_0$ is the photon energy, and $\hbar g$ is the coupling constant between the photon and the two level system, together with the pseudospin Hamiltonian

$$H_{\text{spin}} = \hbar\omega_s \left(\sum_{\alpha=1}^N \sigma_{\alpha}^{+} \sigma_{\alpha}^{-} - 1 \right) - \sum_{\langle \alpha, \beta \rangle} J_{\alpha\beta} (\sigma_{\alpha}^{-} \sigma_{\beta}^{+} + \sigma_{\alpha}^{+} \sigma_{\beta}^{-}), \quad (2)$$

where α and β are the indices of atoms, $\langle\alpha, \beta\rangle$ stands for the nearest-neighbor sites, σ_α^+ (σ_α^-) is a pseudospin raising (lowering) operator describing the two levels of the atom α , and $J_{\alpha\beta}$ is the exchange coupling constant. We have subtracted the energy of the single pseudospin $\hbar\omega_s$ in (2). The Hamiltonian (1) is called the Jaynes-Cummings model [44] without the exchange interaction terms ($J_{\alpha\beta} = 0$). The exchange interaction terms are realized based on superconducting qubits [40,41], about which we review in the Appendix.

The total number N_{total} defined by

$$N_{\text{total}} = \hat{a}^\dagger \hat{a} + \sum_{\alpha=1}^N \sigma_\alpha^+ \sigma_\alpha^- \quad (3)$$

is a conserved quantity, $[H_{\text{total}}, N_{\text{total}}] = 0$. We consider the case $N_{\text{total}} = 1$. A single photon can be experimentally prepared [45–48]. In this case, the system (1) together with (2) is equivalently described by the bosonic Hamiltonian

$$H_{\text{boson}} = - \sum_{(\alpha, \beta)} J_{\alpha\beta} (\hat{b}_\alpha^\dagger \hat{b}_\beta + \hat{b}_\beta^\dagger \hat{b}_\alpha) + \hbar\omega_s \sum_{\alpha=1}^N \hat{b}_\alpha^\dagger \hat{b}_\alpha + \hbar g \sum_{\alpha=1}^N (\hat{a}^\dagger \hat{b}_\alpha + \hat{b}_\alpha^\dagger \hat{a}) + \hbar\omega_0 \hat{a}^\dagger \hat{a} - \hbar\omega_s, \quad (4)$$

where the use is made of the relations [49,50],

$$\begin{aligned} \sigma_\alpha^- \sigma_\beta^+ &= \hat{b}_\beta^\dagger \hat{b}_\alpha, & \sigma_\alpha^+ \sigma_\beta^- &= \hat{b}_\alpha^\dagger \hat{b}_\beta, \\ \hat{a}^\dagger \sigma_\alpha^- &= \hat{a}^\dagger \hat{b}_\alpha, & \hat{a} \sigma_\alpha^+ &= \hat{b}_\alpha^\dagger \hat{a}. \end{aligned} \quad (5)$$

The photon couples equally with each atom with the coupling strength $\hbar g$ in (4), which implies that the additional coupling due to the photon is highly nonlocal. Hence, it is a nontrivial problem whether topological properties keep to hold in the presence of the coupling with a photon.

We argue that the eigenenergy depends on the photon energy $\hbar\omega_0$ through the combination

$$\hbar\Delta\omega \equiv \hbar\omega_0 - \hbar\omega_s, \quad (6)$$

because it appears only in the diagonal term of the Hamiltonian (4) as

$$\hbar\omega_s \sum_{\alpha=1}^N \hat{b}_\alpha^\dagger \hat{b}_\alpha + \hbar\omega_0 \hat{a}^\dagger \hat{a} - \hbar\omega_s. \quad (7)$$

Its eigenvalue is $\hbar\Delta\omega$ when $\hat{a}^\dagger \hat{a} = 1$ and $\sum_{\alpha=1}^N \hat{b}_\alpha^\dagger \hat{b}_\alpha = 0$, while it is zero when $\hat{a}^\dagger \hat{a} = 0$ and $\sum_{\alpha=1}^N \hat{b}_\alpha^\dagger \hat{b}_\alpha = 1$. Hence, the energy depends only on $\hbar\Delta\omega$ although there are two independent energies $\hbar\omega_0$ and $\hbar\omega_s$ in the Hamiltonian.

III. PHOTON LOSS

Because the cavity is an open quantum system it is necessary to include the effect of the photon loss. The Lindblad equation for the density matrix ρ reads

$$\frac{d\rho}{dt} = -\frac{i}{\hbar} [H_{\text{total}}, \rho] + \gamma \left(L\rho L^\dagger - \frac{1}{2} \{L^\dagger L, \rho\} \right), \quad (8)$$

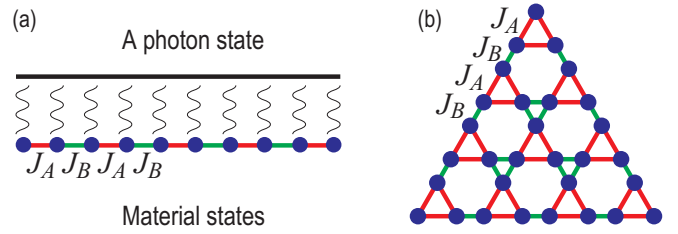


FIG. 1. (a) Illustration of the SSH model with each site equally coupled with a single photon. (b) That of the breathing kagome lattice.

where L is the Lindblad operator describing the dissipation γ . This equation is rewritten in the form of

$$\frac{d\rho}{dt} = -\frac{i}{\hbar} (H_{\text{eff}}\rho - \rho H_{\text{eff}}^\dagger) + \gamma L\rho L^\dagger, \quad (9)$$

where H_{eff} is a non-Hermitian effective Hamiltonian defined by

$$H_{\text{eff}} \equiv H_{\text{total}} - \frac{i\hbar\gamma}{2} L^\dagger L. \quad (10)$$

The photon loss is described by the Lindblad operator as $L = \hat{a}$. The non-Hermitian effective Hamiltonian together with the photon loss term reads

$$H_{\text{eff}} \equiv H_{\text{total}} - \frac{i\hbar}{2} \gamma \hat{a}^\dagger \hat{a}. \quad (11)$$

The imaginary part of the energy spectrum is proportional to the photon number ($\hat{a}^\dagger \hat{a}$), where the dissipation occurs only in the photon state in the present model.

IV. CAVITY-COUPLED SSH MODEL

A. Model

By setting $J_{\alpha\beta} = J_A$ or J_B alternatively in a one-dimensional chain as illustrated in Fig. 1(a), we obtain the dimerized XX model [51–53],

$$\begin{aligned} H_{\text{spin-SSH}} = & - \sum_{\alpha} [J_A (\sigma_{2\alpha-1}^- \sigma_{2\alpha}^+ + \sigma_{2\alpha-1}^+ \sigma_{2\alpha}^-) \\ & + J_B (\sigma_{2\alpha}^- \sigma_{2\alpha+1}^+ + \sigma_{2\alpha}^+ \sigma_{2\alpha+1}^-)] \\ & + \hbar\omega_s \left(\sum_{\alpha=1}^N \frac{\sigma_\alpha^+ \sigma_\alpha^-}{2} - 1 \right), \end{aligned} \quad (12)$$

from the interaction part of the Hamiltonian (2). The corresponding bosonic Hamiltonian together with the photon coupling and the photon loss reads

$$\begin{aligned} H_{\text{cavity-SSH}} = & \hbar\omega_0 \hat{a}^\dagger \hat{a} - \sum_{\alpha} [J_A (\hat{b}_{2\alpha-1}^\dagger \hat{b}_{2\alpha} + \hat{b}_{2\alpha}^\dagger \hat{b}_{2\alpha-1}) \\ & + J_B (\hat{b}_{2\alpha}^\dagger \hat{b}_{2\alpha+1} + \hat{b}_{2\alpha+1}^\dagger \hat{b}_{2\alpha}) + \hbar g (\hat{a}^\dagger \hat{b}_\alpha + \hat{b}_\alpha^\dagger \hat{a})] \\ & + \sum_{\alpha=1}^N \hbar\omega_s \hat{b}_\alpha^\dagger \hat{b}_\alpha - \hbar\omega_s - \frac{i\hbar}{2} \gamma \hat{a}^\dagger \hat{a}. \end{aligned} \quad (13)$$

This is the basic Hamiltonian that we analyze. We set

$$J_A = J(1 + \lambda), \quad J_B = J(1 - \lambda) \quad (14)$$

with λ the dimerization. We take $\hbar\gamma/J = 0.2$ in numerical simulations throughout the paper.

In the absence of the photon coupling ($g = 0$), the Hamiltonian matrix is identical to the SSH model. The system is trivial for $|J_A| > |J_B|$ ($\lambda > 0$) and topological for $|J_A| < |J_B|$ ($\lambda < 0$). This is correct even in the presence of the photon coupling ($g \neq 0$), about which we prove in the next subsection.

B. Topological number

We show how to calculate the topological number in the SSH system coupled with a photon. The Hamiltonian in the momentum space reads

$$\hat{H}(k) = \hat{\psi}^\dagger \begin{pmatrix} 0 & -(J_A + J_B e^{-iak}) & \hbar g \delta(k) \\ -(J_A + J_B e^{-iak}) & 0 & \hbar g \delta(k) \\ \hbar g \delta(k) & \hbar g \delta(k) & \hbar \Delta \omega \end{pmatrix} \hat{\psi} \quad (15)$$

with

$$\hat{\psi} = \begin{pmatrix} \hat{b}_A \\ \hat{b}_B \\ \hat{a} \end{pmatrix}. \quad (16)$$

The winding number for the boson \hat{b}_α is given by

$$W \equiv \frac{1}{2\pi ai} \int_0^{2\pi} \langle \psi_b | \frac{d}{dk} | \psi_b \rangle dk, \quad (17)$$

where $|\psi_b\rangle$ is the right eigenfunction and $\langle \psi_b |$ is the left eigenfunction of the boson \hat{b}_α . We separate it as

$$W \equiv W_1 + W_2 + W_3, \quad (18)$$

$$W_1 \equiv \frac{1}{2\pi ai} \lim_{\varepsilon \rightarrow 0} \int_\varepsilon^{2\pi-\varepsilon} \langle \psi_b | \frac{d}{dk} | \psi_b \rangle dk, \quad (19)$$

$$W_2 \equiv \frac{1}{2\pi ai} \lim_{\varepsilon \rightarrow 0} \int_0^\varepsilon \langle \psi_b | \frac{d}{dk} | \psi_b \rangle dk, \quad (20)$$

$$W_3 \equiv \frac{1}{2\pi ai} \lim_{\varepsilon \rightarrow 0} \int_{2\pi-\varepsilon}^{2\pi} \langle \psi_b | \frac{d}{dk} | \psi_b \rangle dk, \quad (21)$$

and calculate each term.

First, W_1 is calculated by using the eigenfunction of the two-band Hamiltonian

$$H(k) = - \begin{pmatrix} 0 & J_A + J_B e^{-iak} \\ J_A + J_B e^{-iak} & 0 \end{pmatrix}, \quad (22)$$

which is identical to the original SSH model. Eigenenergies are

$$E(k) = \pm \sqrt{J_A^2 + J_B^2 + 2J_A J_B \cos ak}, \quad (23)$$

and the eigenfunctions are

$$\psi(k) = \frac{1}{\sqrt{2}} \left(1, \mp \frac{J_A + J_B e^{iak}}{|E(k)|} \right). \quad (24)$$

Hence, we have $W_1 = 1$ for the topological phase ($|J_A| < |J_B|$) and $W_1 = 0$ for the trivial phase ($|J_A| > |J_B|$).

Next, W_2 is calculated by rewriting (20) as

$$W_2 \equiv \frac{1}{2\pi ai} \lim_{\varepsilon \rightarrow 0} \varepsilon \langle \psi_b | \psi_b \rangle dk, \quad (25)$$

where $|\psi_b\rangle$ is the eigenfunction of (22) and $\langle \psi_b |$ is the eigenfunction of

$$H(0) = \begin{pmatrix} 0 & -(J_A + J_B) & \hbar g \\ -(J_A + J_B) & 0 & \hbar g \\ \hbar g & \hbar g & \hbar \Delta \omega \end{pmatrix}, \quad (26)$$

where the eigenenergies are

$$E_{\pm}(0) = \frac{-(J_A + J_B) + \hbar \Delta \omega \pm \sqrt{(J_A + J_B + \hbar \Delta \omega)^2 + 8\hbar^2 g^2}}{2},$$

$$E_0(0) = J_A + J_B, \quad (27)$$

and the corresponding eigenfunctions are

$$\psi_{\pm}(0) = \frac{1}{\sqrt{1 + 2|f_{\pm}|^2}} (f_{\pm}, f_{\pm}, 1), \quad (28)$$

$$\psi_0(0) = \frac{1}{\sqrt{2}} (-1, 1, 0), \quad (29)$$

with

$$f_{\pm} \equiv \frac{J_A + J_B - \hbar \Delta \omega \pm \sqrt{(J_A + J_B - \hbar \Delta \omega)^2 + 8\hbar^2 g^2}}{4\hbar g}. \quad (30)$$

We take the part of boson \hat{b} , which is given by

$$\psi(0) = \frac{1}{\sqrt{2}} (1, 1). \quad (31)$$

We have the finite inner product

$$\lim_{\varepsilon \rightarrow +0} \langle \psi_b(\varepsilon) | \psi_b(0) \rangle = 1, \quad (32)$$

and hence, we obtain $W_2 = 0$. In the similar way, we have $W_3 = 0$.

As a result, we conclude $W = 1$ for the topological phase ($|J_A| < |J_B|$) and $W = 0$ for the trivial phase ($|J_A| > |J_B|$). Hence, there is no topological phase transition induced by the photon coupling.

C. Band structure

We show the energy spectrum for $g = 0$ as a function of λ in Fig. 2(a), where we have chosen $\Delta\omega < 0$ as a typical case, with $\Delta\omega$ defined by Eq. (6). In the trivial phase ($\lambda > 0$), there is no zero-energy edge state. In the topological phase ($\lambda < 0$), there are two zero-energy edge states localized at the left and right edges. They form the symmetric state and the antisymmetric state under reflection. The photon state is present as indicated by a red line parallel to the λ axis.

The energy spectrum is given for $g \neq 0$ as a function of λ in Figs. 2(b) and 2(c). For $\lambda < 0$, the symmetric topological edge state slightly acquires a nonzero energy due to the photon coupling, while the antisymmetric topological edge state remains precisely at zero energy because the antisymmetric state does not couple with the photon. Furthermore, for all λ , one flat state is detached from the bulk band, which we call the detached state. It is essentially the same one that is known in the Jaynes-Cummings model [54,55].

The photon couples with the symmetric bulk state in the Hamiltonian (13), and its energy changes as indicated by a red line tilted slightly against the λ axis.

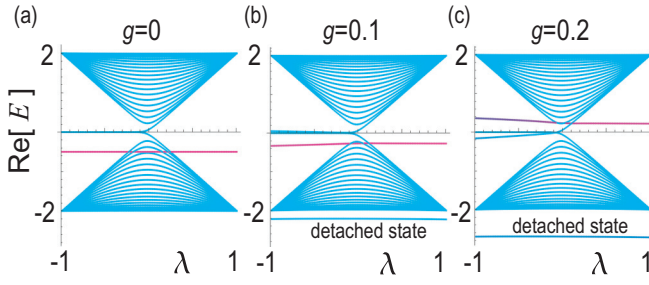


FIG. 2. Energy spectrum as a function of λ , describing bulk bands in cyan, the topological edges in cyan and the photon in red. (a) $\hbar g/J = 0$, (b) $\hbar g/J = 0.1$, and (c) $\hbar g/J = 0.2$. The vertical axis is the energy in units of J . The color of each curve represents the photon number according to the color pallet given in Fig. 3(d). We have set the site number $N = 80$. Note that we have used the abbreviation g instead of $\hbar g/J$ in figures for brevity. This is the case for other figures.

We show the energy spectrum as a function of g in Fig. 3, by taking $\lambda = \pm 0.5$ and $\hbar\Delta\omega$ in the gap between the two bulk bands as in Figs. 3(a1) and 3(b1) as a concrete example. We show the energy spectra for other choices of $\hbar\Delta\omega$ in Fig. 6 below for the sake of completeness.

D. Trivial phase

We examine the trivial phase, where the spectrum consists of four parts, one photon state, two bulk bands and one detached state. See Figs. 3(a1) and 3(a2). The energy of the photon state increases monotonously, while the energy of the detached state decreases monotonously as in Fig. 3(a). We make an analytical study of the spectra of the detached state and the photon state later in Sec. III F, whose result is shown in Fig. 3(c).

E. Polariton and topological edge state

We are interested in the evolution of the symmetric edge state and the photon state as g increases in the topological phase. We show their energy spectra as a function of g in Figs. 3(b1)–(b3) and their wavefunctions for typical values of g in Fig. 4, where we have set $\lambda = -0.5$. Note that the wavefunction can be chosen real.

An anticrossing of these two states occurs at the critical coupling g_c , which is identified by the crossing point in the imaginary energy spectrum [Fig. 3(b2)]. An enlarged picture of the anticrossing structure in the real energy spectrum is shown in Fig. 3(b3), where we observe three branches, the positive-energy branch, the zero-energy branch, and the negative-energy branch. For each state we calculate the photon number $\langle \hat{a}^\dagger \hat{a} \rangle$, which we show in Figs. 3(b4) and 3(f), where red and cyan indicate $\langle \hat{a}^\dagger \hat{a} \rangle = 1$ and $\langle \hat{a}^\dagger \hat{a} \rangle = 0$, respectively, as in the color pallet in Fig. 3(d). In Figs. 3(b4) and 3(f), we find two polaritons transformed smoothly from the edge state and the detached state.

First, we focus on the positive-energy branch, which starts from the symmetric zero-energy edge state at $g = 0$. As g increases, its energy remains almost zero below the anticrossing point ($g < g_c$), but becomes positive and larger for

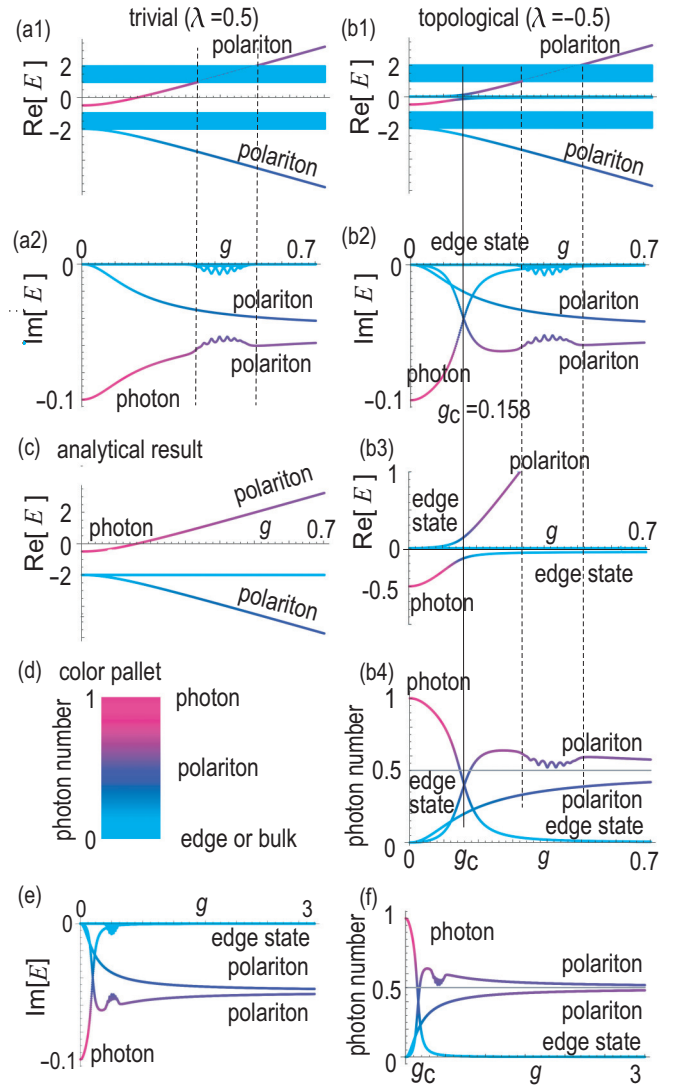


FIG. 3. Energy spectrum as a function of the coupling strength g in the trivial phase with $\lambda = 0.5$ for (a1) and (a2) and in the topological phase with $\lambda = -0.5$ for (b1)–(b3). The photon energy is taken so that $\hbar\Delta\omega \equiv \hbar(\omega_0 - \omega_s) = -0.5J$. (b3) A detailed band structure at the anticrossing point in the topological phase, where there are three branches, the positive-energy branch, the zero-energy branch, and the negative-energy branch. The vertical axis is the energy in units of J . (b4)–(f) The photon number $\langle \hat{a}^\dagger \hat{a} \rangle$ as a function of the coupling strength g in each state, where $\hbar g/J \leq 0.7$ in (b4) and $\hbar g/J \leq 3$ in (f). The photon number turns out to be $1/2$ both for the edge polariton and the detached polariton. (c) Analytical result of Eq. (33). (d) Color pallet showing the photon number. This color pallet is used for all figures. We have set the site number $N = 80$.

$g > g_c$, as in Figs. 3(b1) and 3(b3). Naturally, the edge state at $g = 0$ contains no photon. However, as g approaches g_c and also for $g > g_c$, significant hybridization occurs between the edge state and the photon field, and the hybridized edge state contains a considerable amount of the photon number as in Fig. 3(b4). We show the photon number of the hybridized edge state in a wide range of g , $0 \leq \hbar g/J \leq 3$ in Fig. 3(f), where it is found to approach to $1/2$ as g increases. Such a state is a polariton.

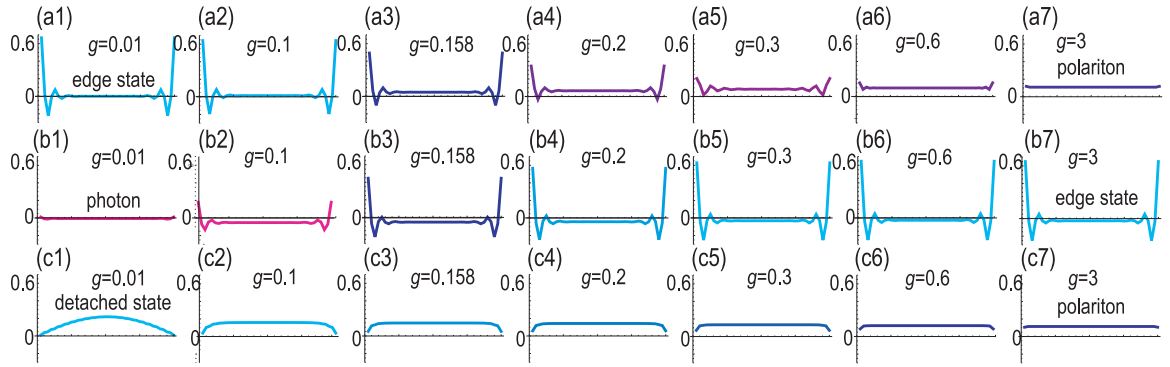


FIG. 4. (a1)–(a7) The wavefunction in the positive-energy branch starting from the edge state toward a polariton state for various g . (b1)–(b7) The wavefunction in the negative-energy branch starting from the photon state toward the edge state for various g . (c1)–(c7) The wavefunction of the detached state starting from a bulk state toward a polariton state for various g . The horizontal axis is the site index from 1 to 80, with the site number $N = 80$. We have considered the topological phase ($\lambda = -0.5$). The anticrossing point is $\hbar g_c/J = 0.158$. The color pallet is is given in Fig. 3(d), which indicates the photon number in each state.

We examine the wavefunction in the positive-energy branch in Figs. 4(a1)–4(a7), where the sign at the bulk site ($\alpha = L/2$) is positive. The polariton state extends over the sample coupled with edge states especially around $\hbar g/J = 0.2$. These properties are reminiscent of the photon and the topological edges. Consequently, as g increases, the symmetric topological edge state is transformed smoothly into the polariton state coupled with the edge state.

Second, the zero-energy branch contains only the antisymmetric topological edge state, which is independent of the coupling constant g .

Third, we focus on the negative-energy branch, which starts from a pure photon state at $g = 0$. As g increases, its energy increases toward zero around the anticrossing point g_c , and becomes almost zero for $g > g_c$, as in Figs. 3(b1) and 3(b3). Naturally, the photon number is 1 at $g = 0$. As g increases, the photon number decreases and eventually becomes zero as in Fig. 3(b4). We examine the wavefunction in the negative-energy branch in Figs. 4(b1)–4(b7), where the sign at the bulk site ($\alpha = L/2$) is negative. The photon state becomes a polariton state coupled with edges around the critical point $\hbar g_c/J = 0.158$, and turns into the edge state around $\hbar g/J = 0.3$. Namely, as g increases, the photon state is transformed smoothly into the symmetric edge state via a polariton state.

The negative-energy branch contains the detached state as well. It couples with the photon. We show the photon number of the hybridized detached state in a wide range of g , $0 \leq$

$\hbar g/J \leq 3$ in Fig. 3(f), where it is found to approach to $1/2$ as g increases. Such a state is also a polariton.

The wavefunction of the detached state is shown in Figs. 4(c1)–4(c7). For small g , it is a bulk state. As the increase of g , it becomes a polariton.

On the other hand, the structures of the two bulk bands is independent of the coupling constant g . In particular, the bulk gap does not close, and hence, the topological properties are robust.

F. Analytic study

It is intriguing that one bulk state is detached from the bulk band due to the interaction with a photon both in the trivial and topological phases as in Figs. 3(a1) and 3(b1). In order to understanding this phenomenon analytically, we make a study of a simple model, where the bulk states collapse to N -fold states at the energy $-2J$ and couple with one photon equally. The energy spectrum is analytically obtained as

$$E/\hbar = -2J + \frac{\Delta\omega - i\gamma/2 \pm \sqrt{(\Delta\omega - i\gamma/2)^2 + 4Ng^2}}{2}, \quad (33)$$

together with $N - 1$ zero-energy level. It is plotted as a function of g in Fig. 3(c). These curves well explain the numerically obtained the energy spectrum in Figs. 3(a1) and 3(b1).

By solving $E = 0$ in Eq. (33), the critical coupling is analytically obtained as

$$g_c = \sqrt{\frac{2J\Delta\omega}{N}}. \quad (34)$$

It well agrees with the numerical result as shown in Fig. 5(a).

The rotating wave approximation requires the conditions $\hbar g \ll \hbar\omega_0$ and $\hbar g \ll \hbar\omega_s$. In the present model calculation, the critical coupling $\hbar g_c/J = 0.158$ may be too strong physically, where the validity of the rotating wave approximation may not be justified. The critical coupling g_c can be tuned by controlling the photon energy $\hbar\omega_0$ as in Fig. 5(a). It is possible to choose an arbitrary small g_c because $g_c = 0$ for $\omega_0 = \omega_s$. For instance, when we choose $\hbar\Delta\omega = -0.1J$, the anticrossing

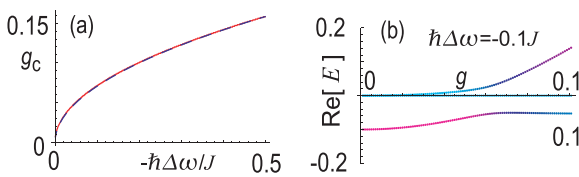


FIG. 5. (a) The critical coupling constant $\hbar g_c$ as a function of the photon energy $-\hbar\Delta\omega$. The red curve indicates the numerical result, while blue curve indicates the analytical result. (b) Energy spectrum as a function of the coupling strength g . The photon energy $\hbar\Delta\omega = -0.1J$. The anticrossing point is $\hbar g_c/J = 0.07$.

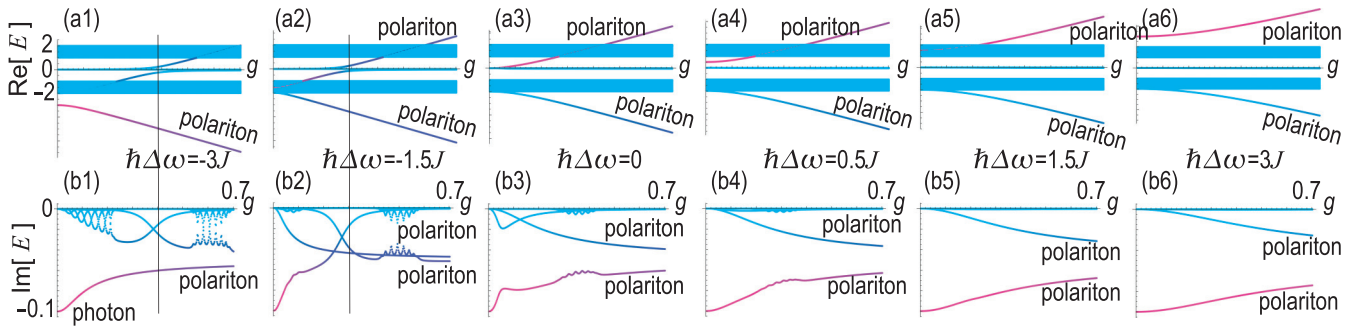


FIG. 6. Energy spectrum as a function of the coupling strength g for various photon energy $\hbar\Delta$. The photon energy is (a) $\hbar\Delta\omega = -3J$, (b) $\hbar\Delta\omega = -1.5J$, (c) $\hbar\Delta\omega = 0$, (d) $\hbar\Delta\omega = 0.5J$, (e) $\hbar\Delta\omega = 1.5J$, and (f) $\hbar\Delta\omega = 3J$.

point is $\hbar g_c/J = 0.07$; see Fig. 5(b). However, we have made a choice of the parameters to make clear the phenomena in this paper.

G. Strong-coupling limit

In the strong-coupling limit ($g \rightarrow \infty$), the hopping parameter can be neglected and the effective Hamiltonian is simply given by

$$H_g = \hbar g \sum_{\alpha=1}^N (\hat{a}^\dagger \hat{b}_\alpha + \hat{b}_\alpha^\dagger \hat{a}). \quad (35)$$

The Hamiltonian is $(N+1) \times (N+1)$ matrix. The eigenenergies are $E_g = \pm\sqrt{N}\hbar g$ and $(N-1)$ -fold degenerate zero energy, as agrees with Eq. (33) in the limit $g \rightarrow \infty$. The eigenfunction corresponding to $E_g = \pm\sqrt{N}\hbar g$ is

$$\psi = \{1/\sqrt{N}, 1/\sqrt{N}, \dots, 1/\sqrt{N}, \pm 1\}/\sqrt{2}, \quad (36)$$

where the first N components are qubit eigenstates and the last component is photon eigenstate. The eigenstate with $E_g = \sqrt{N}\hbar g$ describes the polariton hybridized with the edge state, while the one with $E_g = -\sqrt{N}\hbar g$ describes the polariton hybridized with the detached state. Each of them has the photon number $1/2$. These results are confirmed numerically in Fig. 3(f). Correspondingly, the imaginary parts of the polariton and the edge state approach -0.05 as shown in Fig. 3(e), which is one half of the loss.

H. Photon energy dependence

We show energy spectra as a function of the coupling strength g for various photon energy $\hbar\Delta\omega$ in Fig. 6. The critical coupling constant $g_c = 0$ for $\hbar\Delta\omega = 0$ as in Fig. 6(a3). There are no anticrossing between the photon band and the edge states for $\hbar\Delta\omega > 0$ as shown in Figs. 6(a4)–6(a6).

V. CAVITY-COUPLED KAGOME SECOND-ORDER TOPOLOGICAL INSULATOR

We next analyze the breathing kagome XX model as illustrated in Fig. 1(b), which is a generalization of the dimerized XX model to the breathing kagome lattice. The breathing kagome lattice is composed of the sublattices A and B . The XX interaction exists between the nearest-neighboring sites in the breathing kagome lattice, where the trimerized hopping

J_A and J_B are defined in Fig. 1(b). The Hamiltonian is given by

$$\begin{aligned} H_{\text{spin-Kagome}} = & - \sum_{\langle \alpha \in A, \beta \in B \rangle} [J_A(\sigma_\alpha^- \sigma_\beta^+ + \sigma_\alpha^+ \sigma_\beta^-) \\ & + J_B(\sigma_\beta^- \sigma_\alpha^+ + \sigma_\beta^+ \sigma_\alpha^-)] \\ & + \hbar\omega_s \left(\sum_{\alpha=1}^N \frac{\sigma_\alpha^+ \sigma_\alpha^-}{2} - 1 \right), \end{aligned} \quad (37)$$

where $\langle \alpha \in A, \beta \in B \rangle$ stands for the nearest-neighboring hoppings in the breathing kagome lattice shown in Fig. 1(b). We introduce the trimerization parameter λ as in Eq. (14).

The corresponding Hamiltonian is a second-order topological insulator model [9] with the photon coupling and the photon loss,

$$\begin{aligned} H_{\text{cavity-Kagome}} = & \hbar\omega_0 \hat{a}^\dagger \hat{a} + \hbar\omega_s \sum_{\alpha} \hat{b}_\alpha^\dagger \hat{b}_\alpha - \hbar\omega_s \\ & - \sum_{\langle \alpha \in A, \beta \in B \rangle} [J_A(\hat{b}_\alpha^\dagger \hat{b}_\beta + \hat{b}_\beta^\dagger \hat{b}_\alpha) + J_B(\hat{b}_\beta^\dagger \hat{b}_\alpha + \hat{b}_\alpha^\dagger \hat{b}_\beta)] \\ & + \hbar g \sum_{\alpha} (\hat{a}^\dagger \hat{b}_\alpha + \hat{b}_\alpha^\dagger \hat{a}) - \frac{i\hbar}{2} \gamma \hat{a}^\dagger \hat{a}. \end{aligned} \quad (38)$$

This is the basic Hamiltonian.

The unit cell contains three atoms, which is depicted by red triangles in Fig. 1(b). In the momentum space, the Hamiltonian is given by

$$H = - \begin{pmatrix} 0 & h_{12} & h_{13} & \hbar g \delta(k) \\ h_{12}^* & 0 & h_{23} & \hbar g \delta(k) \\ h_{13}^* & h_{23}^* & 0 & \hbar g \delta(k) \\ \hbar g \delta(k) & \hbar g \delta(k) & \hbar g \delta(k) & \hbar \Delta\omega \end{pmatrix}, \quad (39)$$

with

$$h_{12} = J_A e^{i(k_x/2 + \sqrt{3}k_y/2)} + J_B e^{-i(k_x/2 + \sqrt{3}k_y/2)}, \quad (40)$$

$$h_{23} = J_A e^{i(k_x/2 - \sqrt{3}k_y/2)} + J_B e^{i(-k_x/2 + \sqrt{3}k_y/2)}, \quad (41)$$

$$h_{13} = J_A e^{ik_x} + J_B e^{-ik_x}. \quad (42)$$

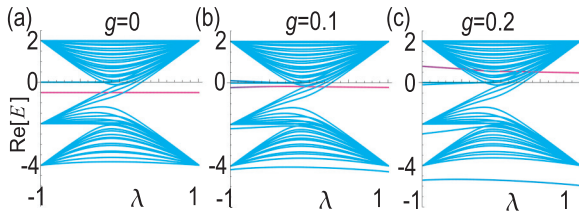


FIG. 7. Energy spectrum as a function of λ in the breathing kagome model, describing three bulk bands in cyan, the topological corners in cyan and the photon in red. (a) $\hbar g/J = 0$, (b) $\hbar g/J = 0.1$, and (c) $\hbar g/J = 0.2$. The vertical axis is the energy in units of J . A detached state from the bulk band is present in (b) and (c). We have set the site number $N = 108$.

The Hamiltonian

$$H_{\text{Kagome}} = \begin{pmatrix} 0 & h_{12} & h_{13} \\ h_{12}^* & 0 & h_{23} \\ h_{13}^* & h_{23}^* & 0 \end{pmatrix} \quad (43)$$

is identical to that of the second-order topological insulator model [9].

The analysis is similarly done as in the cavity-coupled SSH model. The system is trivial for $J_A > J_B$ ($\lambda > 0$) and topological for $J_A < J_B$ ($\lambda < 0$). We show the energy spectrum for $g = 0$ as a function of λ in Fig. 7(a). In the trivial phase ($\lambda > 0$), there is no zero-energy edge state. In the topological phase ($\lambda < 0$), there are three zero-energy topological corner states localized at the three corners. One of them forms the C_3 symmetric state. In addition, the photon state is present as indicated by a red line parallel to the λ axis.

The energy spectrum is given for $g \neq 0$ as a function of λ in Figs. 7(b) and 7(c). For $\lambda < 0$, the C_3 symmetric topological corner state slightly acquires a nonzero energy due to the photon coupling, while the other two topological corner states remain at zero energy. Furthermore, for all λ , one flat state is detached from the bulk band.

We show the energy spectrum as a function of the coupling constant g in Fig. 8. For definiteness, we take the photon energy $\hbar(\omega_0 - \omega_s)$ in the gap between the two bulk bands near the zero-energy level as in Figs. 8(a1) and 8(b1). In the trivial phase the spectrum consists four parts, one photon state, two bulk bands and one detached state; see Figs. 8(a1) and 8(a2). The energy of the photon state increases monotonously while the energy of the detached state decreases monotonously.

On the other hand, in the topological phase the photon state anticrosses the C_3 symmetric corner state as in Fig. 8(b1). The anticrossing point g_c in the real energy spectrum is identified from the crossing point in the imaginary energy spectrum as in Fig. 8(b2). A detailed structure of the anticrossing is very similar to the one in the SSH model shown in Fig. 3(b3). We observe three branches, the positive-energy branch, the zero-energy branch, and the negative-energy branch. The main difference is that there are two zero-energy corner states in the zero-energy branch. In the positive-energy branch, the C_3 symmetric edge state is transformed into a polariton coupled with the corner state as g increases. In the negative-energy branch, the photon state is transformed eventually into the C_3 symmetric topological zero-energy edge state as g increases. The detached state is transformed into a polariton as well.

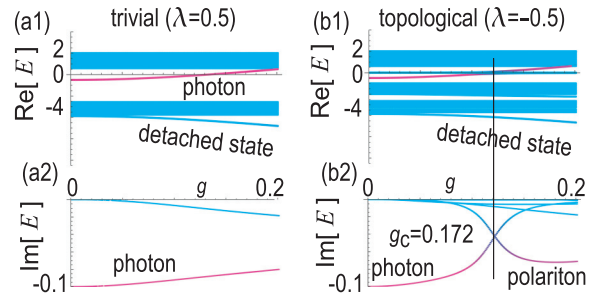


FIG. 8. Energy spectrum of the breathing kagome model as a function of the coupling strength g in the trivial phase with $\lambda = 0.5$ for (a1) and (a2) and in the topological phase with $\lambda = -0.5$ for (b1) and (b2). The photon energy is taken so that $\hbar(\omega_0 - \omega_s) = -0.5J$. The color pallet is the same as in Fig. 3, which indicates the photon number in each state. A detailed band structure around the anticrossing point in the topological phase is almost identical to Fig. 3(b3). The main difference is that the zero-energy branch contains two topological corner states except for the C_3 symmetric one. The vertical axis is the energy in units of J . We have set the site number $N = 108$.

VI. DISCUSSIONS

We have found in the cavity-coupled SSH/kagome model that, as the coupling constant g is increased, the topological edge/corner state is smoothly transformed into a polariton coupled with edge/corner state, while the photon is smoothly transformed into the topological edge/corner state. Because the coupling constant g is continuously controllable [56–58], the experimental observation of these phenomena will be feasible.

The boson numbers ($\hat{b}_\alpha^\dagger \hat{b}_\alpha$) of superconducting qubits are experimentally accessible by quantum nondemolition measurements [59]. On the other hand, the photon number ($\hat{a}^\dagger \hat{a}$) is experimentally observable in superconducting circuits [60].

Another way is the use of magnets, where strong photon-magnon coupling is also realized [31,61,62]. There is a possibility that the present system is realized in magnets. Magnetic moments are represented by spin operators, which correspond to the pseudospin operators in qubits. In the presence of the strong photon-magnon coupling in a cavity, the system Hamiltonian is identical to that of the qubit system. Hence, the topological edge states emerge as in the case of the qubit system. The local spin can be observed by a spin-polarized scanning tunneling microscopy (STM) [63].

We may think of possible applications. Recently, quantum simulation based on qubits is an emerging field of condensed matter physics [64,65]. If we excite a left edge, the wave is propagated along the bulk in the trivial phase because the bulk mode is excited [66,67]. On the other hand, it is not the case in the topological phase because only the localized topological edge mode is excited. Namely, quantum information is transferred in the trivial phase but not in the topological phase. Our results may be useful for topological transfer of information. This will be useful and interesting in future applications of quantum communications and computations.

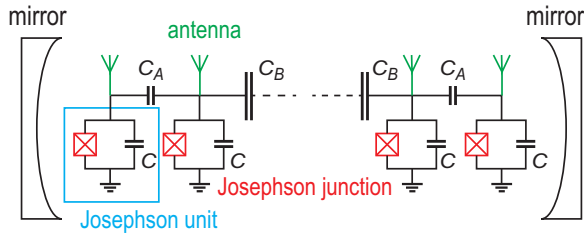


FIG. 9. Illustration of a Josephson circuit. A Josephson unit is composed of a Josephson junction (box with cross) and a shunted capacitance C . A Josephson circuit is a chain of Josephson junctions and alternating capacitances C_A and C_B . An antenna is attached to each Josephson unit. The circuit is set in a cavity composed of two mirrors.

ACKNOWLEDGMENTS

This work is supported by CREST, JST (Grant No. JPMJCR20T2) and Grants-in-Aid for Scientific Research from MEXT KAKENHI (Grant No. 23H00171).

APPENDIX: DERIVATION OF THE EXCHANGE COUPLING IN THE JOSEPHSON CIRCUIT

The exchange interaction terms in the cavity QED Hamiltonian (1) are realized based on superconducting qubits [40,41]. We review the derivation of the exchange coupling in the Josephson circuit [68] illustrated in Fig. 9. We assume that the size of the Josephson circuit is much smaller than that of the cavity, where the coupling is assumed to be a constant g . The Lagrangian of the coupled circuit is

$$\begin{aligned} \mathcal{L}(\Phi_1, \Phi_2, \dot{\Phi}_1, \dot{\Phi}_2) &= \frac{C_1}{2} \dot{\Phi}_1^2 + \frac{C_2}{2} \dot{\Phi}_2^2 + \frac{C_g}{2} (\dot{\Phi}_1 - \dot{\Phi}_2)^2 \\ &+ \frac{I_c \Phi_0}{2\pi} \cos 2\pi \frac{\Phi_1}{\Phi_0} + \frac{I_c \Phi_0}{2\pi} \cos 2\pi \frac{\Phi_2}{\Phi_0}. \end{aligned} \quad (\text{A1})$$

The canonical conjugate momentums are defined by

$$\begin{aligned} Q_1 &\equiv \frac{\partial \mathcal{L}}{\partial \dot{\Phi}_1} = (C_1 + C_g) \dot{\Phi}_1 - C_g \dot{\Phi}_2, \\ Q_2 &\equiv \frac{\partial \mathcal{L}}{\partial \dot{\Phi}_2} = (C_2 + C_g) \dot{\Phi}_2 - C_g \dot{\Phi}_1. \end{aligned} \quad (\text{A2})$$

The corresponding Hamiltonian is calculated as

$$\begin{aligned} \mathcal{H}(Q_1, Q_2, \Phi_1, \Phi_2) &\equiv Q_1 \dot{\Phi}_1 + Q_2 \dot{\Phi}_2 - \mathcal{L} \\ &= ((C_1 + C_g) \dot{\Phi}_1 - C_g \dot{\Phi}_2) \dot{\Phi}_1 \\ &+ ((C_2 + C_g) \dot{\Phi}_2 - C_g \dot{\Phi}_1) \dot{\Phi}_2 \\ &- \left[\frac{C_1}{2} \dot{\Phi}_1^2 + \frac{C_2}{2} \dot{\Phi}_2^2 + \frac{C_g}{2} (\dot{\Phi}_1 - \dot{\Phi}_2)^2 \right. \end{aligned}$$

$$\begin{aligned} &+ \frac{I_c \Phi_0}{2\pi} \cos 2\pi \frac{\Phi_1}{\Phi_0} + \frac{I_c \Phi_0}{2\pi} \cos 2\pi \frac{\Phi_2}{\Phi_0} \left. \right] \\ &= \frac{C_1}{2} \dot{\Phi}_1^2 + \frac{C_2}{2} \dot{\Phi}_2^2 + \frac{C_g}{2} (\dot{\Phi}_1 - \dot{\Phi}_2)^2 \\ &- \frac{I_c \Phi_0}{2\pi} \cos 2\pi \frac{\Phi_1}{\Phi_0} - \frac{I_c \Phi_0}{2\pi} \cos 2\pi \frac{\Phi_2}{\Phi_0}. \end{aligned} \quad (\text{A3})$$

The inverse solutions of Eq. (A2) are

$$\begin{aligned} \dot{\Phi}_1 &= \frac{(C_2 + C_g) Q_1 + C_g Q_2}{C_1 C_2 + C_1 C_g + C_2 C_g}, \\ \dot{\Phi}_2 &= \frac{C_g Q_2 - (C_1 + C_g) Q_1}{C_1 C_2 + C_1 C_g + C_2 C_g}. \end{aligned} \quad (\text{A4})$$

By inserting them, the Hamiltonian reads

$$\begin{aligned} \mathcal{H}(Q_1, Q_2, \Phi_1, \Phi_2) &= \frac{Q_1^2}{2\tilde{C}_1} + \frac{Q_2^2}{2\tilde{C}_2} - \frac{I_c \Phi_0}{2\pi} \cos 2\pi \frac{\Phi_1}{\Phi_0} \\ &- \frac{I_c \Phi_0}{2\pi} \cos 2\pi \frac{\Phi_2}{\Phi_0} + \frac{Q_1 Q_2}{2\tilde{C}_{\text{int}}}, \end{aligned} \quad (\text{A5})$$

with

$$\begin{aligned} \tilde{C}_1 &\equiv \frac{C_1 C_2 + C_2 C_g + C_2 C_g}{C_2 + C_g}, \\ \tilde{C}_2 &\equiv \frac{C_1 C_2 + C_1 C_g + C_2 C_g}{C_1 + C_g}, \\ \tilde{C}_{\text{int}} &\equiv \frac{C_1 C_2 + C_2 C_g + C_2 C_g}{2C_g}. \end{aligned} \quad (\text{A6})$$

The quantized Hamiltonian is

$$\begin{aligned} H &= 4E_N (n - N_g)^2 \hat{a}^\dagger \hat{a} - \frac{E_J}{2} (\hat{a}^\dagger + \hat{a}) \\ &+ 4E_N (n - N_g)^2 \hat{b}^\dagger \hat{b} - \frac{E_J}{2} (\hat{b}^\dagger + \hat{b}) \\ &+ J_{\text{int}} (\hat{a}^\dagger - \hat{a}) (\hat{b}^\dagger - \hat{b}). \end{aligned} \quad (\text{A7})$$

We project it to the two-level model

$$\begin{aligned} H &= \left(\frac{1}{2} - N_g \right) \sigma_z^{(1)} + \frac{E_J}{2} \sigma_x^{(1)} + \left(N_g^2 - N_g + \frac{1}{2} \right) I_2 \\ &+ \left(\frac{1}{2} - N_g \right) \sigma_z^{(2)} + \frac{E_J}{2} \sigma_x^{(2)} + \left(N_g^2 - N_g + \frac{1}{2} \right) I_2 \\ &+ J_{\text{int}} (\sigma_+^{(1)} - \sigma_-^{(1)}) (\sigma_+^{(2)} - \sigma_-^{(2)}). \end{aligned} \quad (\text{A8})$$

The interaction term

$$H_{\text{int}} = J_{\text{int}} (\sigma_+^{(1)} - \sigma_-^{(1)}) (\sigma_+^{(2)} - \sigma_-^{(2)}) \quad (\text{A9})$$

becomes

$$\begin{aligned} H_{\text{int}} &= -J_{\text{int}} (\sigma_+^{(1)} \sigma_-^{(2)} + \sigma_-^{(1)} \sigma_+^{(2)}) \\ &= -J_{\text{int}} (\sigma_x^{(1)} \sigma_x^{(2)} + \sigma_y^{(1)} \sigma_y^{(2)}), \end{aligned} \quad (\text{A10})$$

by using the rotating-wave approximation. It is the exchange coupling in Eq. (12).

The coupling between the Josephson circuit and the photon is made by attaching antenna as shown in Fig. 9. The Josephson circuit system is set in the two mirrors forming a cavity.

- [1] M. Z. Hasan and C. L. Kane, Colloquium: Topological insulators, *Rev. Mod. Phys.* **82**, 3045 (2010).
- [2] X.-L. Qi and S.-C. Zhang, Topological insulators and superconductors, *Rev. Mod. Phys.* **83**, 1057 (2011).
- [3] W. A. Benalcazar, B. A. Bernevig, and T. L. Hughes, Quantized electric multipole insulators, *Science* **357**, 61 (2017).
- [4] F. Schindler, A. Cook, M. G. Vergniory, and T. Neupert, in *APS March Meeting* (American Physical Society, New Orleans, Louisiana, 2017).
- [5] Y. Peng, Y. Bao, and F. von Oppen, Boundary Green functions of topological insulators and superconductors, *Phys. Rev. B* **95**, 235143 (2017).
- [6] J. Langbehn, Y. Peng, L. Trifunovic, F. von Oppen, and P. W. Brouwer, Reflection-symmetric second-order topological insulators and superconductors, *Phys. Rev. Lett.* **119**, 246401 (2017).
- [7] Z. Song, Z. Fang, and C. Fang, Reflection-symmetric second-order topological insulators and superconductors, *Phys. Rev. Lett.* **119**, 246402 (2017).
- [8] W. A. Benalcazar, B. A. Bernevig, and T. L. Hughes, Electric multipole moments, topological multipole moment pumping, and chiral hinge states in crystalline insulators, *Phys. Rev. B* **96**, 245115 (2017).
- [9] M. Ezawa, Higher-order topological insulators and semimetals on the breathing kagome and pyrochlore lattices, *Phys. Rev. Lett.* **120**, 026801 (2018).
- [10] T. Pellizzari, S. A. Gardiner, J. I. Cirac, and P. Zoller, Decoherence, continuous observation, and quantum computing: A cavity QED model, *Phys. Rev. Lett.* **75**, 3788 (1995).
- [11] A. Imamoglu, D. D. Awschalom, G. Burkard, D. P. DiVincenzo, D. Loss, M. Sherwin, and A. Small, Quantum information processing using quantum dot spins and cavity QED, *Phys. Rev. Lett.* **83**, 4204 (1999).
- [12] J. Ye, D. W. Vernooy, and H. J. Kimble, Trapping of single atoms in cavity QED, *Phys. Rev. Lett.* **83**, 4987 (1999).
- [13] S.-B. Zheng and G.-C. Guo, Efficient scheme for two-atom entanglement and quantum information processing in cavity QED, *Phys. Rev. Lett.* **85**, 2392 (2000).
- [14] A. Blais, R.-S. Huang, A. Wallraff, S. M. Girvin, and R. J. Schoelkopf, Cavity quantum electrodynamics for superconducting electrical circuits: An architecture for quantum computation, *Phys. Rev. A* **69**, 062320 (2004).
- [15] X. Gu, A. F. Kockum, A. Miranowicz, Y.-X. Liu, and F. Nori, Microwave photonics with superconducting quantum circuits, *Phys. Rep.* **718-719**, 1 (2017).
- [16] A. Blais, A. L. Grimsmo, S. M. Girvin, and A. Wallraff, Circuit quantum electrodynamics, *Rev. Mod. Phys.* **93**, 025005 (2021).
- [17] J. Bourassa, J. M. Gambetta, A. A. Abdumalikov, Jr., O. Astafiev, Y. Nakamura, and A. Blais, Ultrastrong coupling regime of cavity QED with phase-biased flux qubits, *Phys. Rev. A* **80**, 032109 (2009).
- [18] T. Niemczyk, F. Deppe, H. Huebl, E. P. Menzel, F. Hocke, M. J. Schwarz, J. J. Garcia-Ripoll, D. Zueco, T. Hummer, E. Solano *et al.*, Circuit quantum electrodynamics in the ultrastrong-coupling regime, *Nat. Phys.* **6**, 772 (2010).
- [19] A. F. Kockum, A. Miranowicz, S. De Liberato, S. Savasta, and F. Nori, Ultrastrong coupling between light and matter, *Nat. Rev. Phys.* **1**, 19 (2019).
- [20] P. Forn-Díaz, L. Lamata, E. Rico, J. Kono, and E. Solano, Ultrastrong coupling regimes of light-matter interaction, *Rev. Mod. Phys.* **91**, 025005 (2019).
- [21] Y. Ashida, A. Imamoglu, and E. Demler, Cavity quantum electrodynamics at arbitrary light-matter coupling strengths, *Phys. Rev. Lett.* **126**, 153603 (2021).
- [22] J. Bloch, A. Cavalleri, V. Galitski, M. Hafezi, and A. Rubio, Strongly correlated electron-photon systems, *Nature (London)* **606**, 41 (2022).
- [23] S. Schmidt and J. Koch, Circuit QED lattices Towards quantum simulation with superconducting circuits, *Ann. Phys. (Berlin)* **525**, 395 (2013).
- [24] G. Calajo, F. Ciccarello, D. Chang, and P. Rabl, Atom-field dressed states in slow-light waveguide QED, *Phys. Rev. A* **93**, 033833 (2016).
- [25] E. Cortese, N.-L. Tran, J.-M. Manceau, A. Bousseksou, I. Carusotto, G. Biasiol, R. Colombelli, and S. De Liberato, Excitons bound by photon exchange, *Nat. Phys.* **17**, 31 (2021).
- [26] D. De Bernardis, Z.-P. Cian, I. Carusotto, M. Hafezi, and P. Rabl, Light-matter interactions in synthetic magnetic fields: Landau-photon polaritons, *Phys. Rev. Lett.* **126**, 103603 (2021).
- [27] D. De Bernardis, M. Jeannin, J.-M. Manceau, R. Colombelli, A. Tredicucci, and I. Carusotto, Magnetic-field-induced cavity protection for intersubband polaritons, *Phys. Rev. B* **106**, 224206 (2022).
- [28] F. Schlawin, D. M. Kennes, and M. A. Sentef, Cavity quantum materials, *Appl. Phys. Rev.* **9**, 011312 (2022).
- [29] F. Schlawin, A. Cavalleri, and D. Jaksch, Cavity-mediated electron-photon superconductivity, *Phys. Rev. Lett.* **122**, 133602 (2019).
- [30] Y. Ashida, A. Imamoglu, J. Faist, D. Jaksch, A. Cavalleri, and E. Demler, Quantum electrodynamic control of matter: Cavity-enhanced ferroelectric phase transition, *Phys. Rev. X* **10**, 041027 (2020).
- [31] O. O. Soykal and M. E. Flatte, Strong field interactions between a nanomagnet, and a photonic cavity, *Phys. Rev. Lett.* **104**, 077202 (2010).
- [32] O. V. Kibis, O. Kyriienko, and I. A. Shelykh, Band gap in graphene induced by vacuum fluctuations, *Phys. Rev. B* **84**, 195413 (2011).
- [33] G. Scalari, C. Maissen, D. Turcinkov, D. Hagenmuller, S. De Liberato, C. Ciuti, C. Reichl, D. Schuh, W. Wegscheider, M. Beck, and J. Faist, Ultrastrong coupling of the cyclotron transition of a 2D electron gas to a THz metamaterial, *Science* **335**, 1323 (2012).
- [34] X. Wang, E. Ronca, and M. A. Sentef, Cavity quantum electrodynamical Chern insulator: Towards light-induced quantized anomalous Hall effect in graphene, *Phys. Rev. B* **99**, 235156 (2019).
- [35] O. Dmytruk and M. Schirò, Controlling topological phases of matter with quantum light, *Commun. Phys.* **5**, 271 (2022).
- [36] B. Pérez-González, Á. Gómez-León, and G. Platero, Topology detection in cavity QED, *Phys. Chem. Chem. Phys.* **24**, 15860 (2022).
- [37] D.-W. Wang, C. Zhao, J. Yang, Y.-T. Yan, and L. Zhou, Simulating the extended Su-Schrieffer-Heeger model, and transferring an entangled state based on a hybrid cavity-magnon array, *Phys. Rev. A* **107**, 053701 (2023).

- [38] D. Shaffer, M. Claassen, A. Srivastava, and L. H. Santos, Entanglement, and topology in Su-Schrieffer-Heeger cavity quantum electrodynamics, *Phys. Rev. B* **109**, 155160 (2024).
- [39] C. A. Downing, T. J. Sturges, G. Weick, M. Stobińska, and L. M. Moreno, Topological phases of polaritons in a cavity waveguide, *Phys. Rev. Lett.* **123**, 217401 (2019).
- [40] W. Nie, Z. H. Peng, F. Nori, and Y. X. Liu, Topologically protected quantum coherence in a superatom, *Phys. Rev. Lett.* **124**, 023603 (2020).
- [41] W. Nie, and Y.-X. Liu, Bandgap-assisted quantum control of topological edge states in a cavity, *Phys. Rev. Res.* **2**, 012076(R) (2020).
- [42] C.-y. Wang, Y.-J. Zheng, M.-S. Wei, M.-J. Liao, Z.-J. Lin, C. Wang, Y.-P. Yang, and J.-P. Xu, Influence of a topological artificial atom chain on the transmission properties of a cavity, *Opt. Express* **31**, 15342 (2023).
- [43] P. Saugmann and J. Larson, A Fock state lattice approach to quantum optics, *Phys. Rev. A* **108**, 033721 (2023).
- [44] E. T. Jaynes and F. W. Cummings, Comparison of quantum, and semiclassical radiation theories with application to the beam maser, *Proc. IEEE* **51**, 89 (1963).
- [45] J. McKeever, A. Boca, A. D. Boozer, R. Miller, J. R. Buck, A. Kuzmich, and H. J. Kimble, Deterministic generation of single photons from one atom trapped in a cavity, *Science* **303**, 1992 (2004).
- [46] M. Keller, B. Lange, K. Hayasaka, W. Lange, and H. Walther, Continuous generation of single photons with controlled waveform in an ion-trap cavity system, *Nature (London)* **431**, 1075 (2004).
- [47] I.-C. Hoi, C. M. Wilson, G. Johansson, T. Palomaki, B. Peropadre, and P. Delsing, Demonstration of a single-photon router in the microwave regime, *Phys. Rev. Lett.* **107**, 073601 (2011).
- [48] L. Scarpelli, B. Lang, F. Masia, D. M. Beggs, E. A. Muljarov, A. B. Young, R. Oulton, M. Kamp, S. Hofling, C. Schneider *et al.*, 99% beta factor, and directional coupling of quantum dots to fast light in photonic crystal waveguides determined by spectral imaging, *Phys. Rev. B* **100**, 035311 (2019).
- [49] H. Bethe, Zur theorie der metalle, *Z. Phys.* **71**, 205 (1931).
- [50] L. Hulthen, Uber das austauschproblem eines kristalles, *Arkiv for matematik, astronomi och fysik* **26A**, 1 (1938).
- [51] J. H. Yaylor and G. Muller, Magnetic field effects in the dynamics of alternating or anisotropic quantum spin chains, *Physica A* **130**, 1 (1985).
- [52] O. Derzhko, T. Krokhnalskii, J. J. Stolze, Dynamic properties of the dimerized spin-isotropic XY chain in a transverse field, *J. Phys. A: Math. Gen.* **35**, 3573 (2002).
- [53] J. Stolze and T. Garske, The emptiness formation probability correlation in homogeneous, and dimerized XX chains, *Condens. Matter Phys.* **12**, 369 (2009).
- [54] D. Braak, Integrability of the Rabi model, *Phys. Rev. Lett.* **107**, 100401 (2011).
- [55] H. Huebl, Christoph W. Zollitsch, J. Lotze, F. Hocke, M. Greifenstein, A. Marx, R. Gross, and T. B. Sebastian Goennenwein, High cooperativity in coupled microwave resonator ferrimagnetic insulator hybrids, *Phys. Rev. Lett.* **111**, 127003 (2013).
- [56] K. M. Fortier, S. Y. Kim, M. J. Gibbons, P. Ahmadi, and M. S. Chapman, Deterministic loading of individual atoms to a high-finesse optical cavity, *Phys. Rev. Lett.* **98**, 233601 (2007).
- [57] M. Khudaverdyan, W. Alt, I. Dotsenko, T. Kampschulte, K. Lenhard, A. Rauschenbeutel, S. Reick, K. Schorner, A. Widera, and D. Meschede, Controlled insertion, and retrieval of atoms coupled to a high-finesse optical resonator, *New J. Phys.* **10**, 073023 (2008).
- [58] S. Kang, Y. Choi, S. Lim, W. Kim, J.-R. Kim, J.-H. Lee, and Ky. An, Continuous control of the coupling constant in an atom-cavity system by using elliptic polarization, and magnetic sublevels, *Opt. Express* **18**, 9286 (2010).
- [59] A. Lupaşcu, S. Saito, T. Picot, P. C. de Groot, C. J. P. M. Harmans, and J. E. Mooij, Quantum non-demolition measurement of a superconducting two-level system, *Nat. Phys.* **3**, 119 (2007).
- [60] D. I. Schuster, A. A. Houck, J. A. Schreier, A. Wallraff, J. M. Gambetta, A. Blais, L. Frunzio, J. Majer, B. Johnson, M. H. Devoret *et al.*, Resolving photon number states in a superconducting circuit, *Nature (London)* **445**, 515 (2007).
- [61] A. Imamoğlu, Cavity QED based on collective magnetic dipole coupling: Spin ensembles as hybrid two-level systems, *Phys. Rev. Lett.* **102**, 083602 (2009).
- [62] R. Amsüss, C. Koller, T. Nauer, S. Putz, S. Rotter, K. Sandner, S. Schneider, M. Schrambock, G. Steinhauser, H. Ritsch, J. Schmiedmayer, and J. Majer, Cavity QED with magnetically coupled collective spin states, *Phys. Rev. Lett.* **107**, 060502 (2011).
- [63] R. Wiesendanger, Spin mapping at the nanoscale, and atomic scale, *Rev. Mod. Phys.* **81**, 1495 (2009).
- [64] I. Buluta and F. Nori, Quantum simulators, *Science* **326**, 108 (2009).
- [65] I. M. Georgescu, S. Ashhab, and F. Nori, Quantum simulation, *Rev. Mod. Phys.* **86**, 153 (2014).
- [66] M. Ezawa, Electric-circuit simulation of the Schrödinger equation, and non-Hermitian quantum walks, *Phys. Rev. B* **100**, 165419 (2019).
- [67] M. Ezawa, Nonlinearity-induced transition in nonlinear Su-Schrieffer-Heeger model, and nonlinear higher-order topological system, *Phys. Rev. B* **104**, 235420 (2021).
- [68] P. Krantz, M. Kjaergaard, F. Yan, T. P. Orlando, S. Gustavsson, and W. D. Oliver, A quantum engineer's guide to superconducting qubits, *Appl. Phys. Rev.* **6**, 021318 (2019).